ARTICLE   **OPEN**

Comprehensive investigation of quantum oscillations in semimetal using an ac composite magnetoelectric technique with ultrahigh sensitivity

Long Zhang[1,2,6], Tianyang Wang[3,6], Yugang Zhang[1,2], Shuang Liu[1], Yuping Sun[3,4,5], Xiaoyuan Zhou[1], Young Sun[1], Mingquan He[1,2], Aifeng Wang[1,2], Xuan Luo[3✉] and Yisheng Chai[1,2✉]

Quantum oscillation (QO), a physical phenomenon that reflects the characteristics of the Fermi surface and transport fermions, has been extensively observed in metals and semimetals through various approaches, like magnetostriction, magnetization, resistivity, and thermoelectric power. However, only limited oscillation frequencies can be revealed by the aforementioned methods, particularly in semimetals with intricate Fermi pockets and associated magnetic breakdown phenomena. In this paper, we present the application of an ac composite magnetoelectric (ME) technique to measure the QOs of a topological nodal-line semimetal, ZrSiS, which possesses six fundamental QO frequencies. By employing the ME technique with a maximum magnetic field of 13 T and a minimum temperature of 2 K, we are able to capture all the fundamental frequencies and most of the permissible magnetic breakdown frequencies. Remarkably, a series of magnetic breakdown frequencies around 8000 T were revealed even in a magnetic field as low as 7.5 T. These findings highlight the ME technique as an ultrahigh-sensitive tool for studying Dirac Fermions and other topological semimetals with complex Fermi surfaces.

INTRODUCTION

In metals or semimetals, application of a strong magnetic field (**B**) at low temperatures (T) leads to the quantization of electronic states into discrete Landau Levels with distinct energies, resulting in periodic oscillations of the density of states near the Fermi surface, dubbed quantum oscillation (QO)[1]. These oscillations were experimentally observed in magnetization and resistivity measurements in bismuth during the 1930s, known as de Haas–van Alphen (dHvA) oscillations and Shubnikov–de Haas (SdH) oscillations, respectively[2,3]. The oscillatory period is traditionally represented in an inverse magnetic field plot. The corresponding frequency (F_r) is proportional to the extremal cross-section of the Fermi surface (A_F) perpendicular to the applied field, as dictated by the Onsager relation $F_r = (\varphi_0/2\pi^2)A_F$, where $\varphi_0 = h/2e$ is the magnetic flux quantum. This characteristic establishes quantum oscillation as one of the most powerful tools for investigating the geometry of Fermi surface.

In recent years, nodal-line semimetals that feature Dirac band crossings as lines or closed loops in momentum space have attracted significant interest as new topological systems[4–9]. Among the experimentally verified nodal-line semimetals, ZrSiS stands out with its strong linear Dirac dispersion spanning an energy range of ~2 eV, indicating the presence of nearly massless transport fermions[6,7]. It is also notable for its intricate Fermi surface configuration and up to six fundamental frequencies: $F(\delta_1) \sim 8.5$ T, $F(\delta_2) \sim 16.5$ T, $F(\gamma_1) \sim 22$ T, $F(\gamma_2) \sim 92$ T, $F(\alpha) \sim 240$ T, $F(\beta) \sim 419$ T. Accordingly, clear QOs have been detected in various physical properties, including resistivity[10–12], magnetization[13], thermopower[14], and magnetic torque[15,16]. Notably, the α and β pockets located on the Z-R-A plane can additionally exhibit the magnetic breakdown phenomena, leading to QO frequencies up to ~8000 T. However, no single method has been successful in fully capturing all these frequencies at temperatures above 2 K and in magnetic fields below 14 T. Moreover, even under high magnetic fields up to 31 T and temperatures as low as 0.4 K, certain frequencies like $F(\beta)$ remained absent in SdH oscillations, which was proposed to be related to specific scattering mechanism[16]. Thus, discrepancies among different studies have only provided fragmented insights into the complete picture of the Fermi surface.

Typically, the magnitude of QOs at a specific frequency increases with declining temperatures and increasing magnetic fields. This can be ascribed to the thermal damping factor $R_T = aT\mu/[B\sinh(aT\mu/B)]$ and the field-related damping factor $R_D = \exp(-aT_D\mu/B)$ in the Lifshitz-Kosevich (LK) formula, respectively[1]. Here, $a = (2\pi^2 k_B m_0)/(\hbar e)$ is a constant, $\mu = m^*/m_0$ represents the relative effective mass, m_0 denotes the mass of a free electron, and T_D is the Dingle temperature. Consequently, to extract comprehensive information about the Fermi surface, investigations of QOs often require extreme conditions including ultralow temperatures (<1 K) and high magnetic fields (>20 T). However, achieving these conditions is challenging with standard cryogenic magnets, which typically operate at relatively moderate temperatures (>1.8 K) and within a limited field range (<14 T). Under these conditions, each measurement technique may only reveal a subset of QO frequencies, like in ZrSiS[11–14]. Currently, there is no single measurement capable of capturing all its quantum oscillation frequencies under general experimental

[1]Center of Quantum Materials and Devices, Chongqing University, Chongqing 401331, China. [2]Low Temperature Physics Laboratory, College of Physics, Chongqing University, Chongqing 401331, China. [3]Key Laboratory of Materials Physics, Institute of Solid State Physics, HFIPS, Chinese Academy of Sciences, Hefei 230031, China. [4]Anhui Province Key Laboratory of Condensed Matter Physics at Extreme Conditions, High Magnetic Field Laboratory, HFIPS, Chinese Academy of Sciences, Hefei 230031, China. [5]Collaborative Innovation Centre of Advanced Microstructures, Nanjing University, Nanjing 210093, China. [6]These authors contributed equally: Long Zhang, Tianyang Wang. ✉email: xluo@issp.ac.cn; yschai@cqu.edu.cn

conditions. Such a comprehensive measurement is highly desirable for exploring the complex and non-trivial Fermiology in semimetals. It would enable us to investigate complete Fermi surfaces in a single attempt, in case the sample orientation varies slightly when combining different methodologies. Therefore, this approach is particularly crucial for samples with Fermi surfaces that are both complex and sensitive to tilting angles.

Recently, we adopted a composite magnetoelectric (ME) technique as a highly sensitive tool for investigating magnetic materials[17–19]. A composite laminate magnetoelectric configuration is used, stemming from renewed interest in room temperature multiferroics from the year 2000[20]. In this method, a thin sample is affixed to a piezoelectric transducer using silver epoxy to form a bilayer composite magnetoelectric laminate. The piezoelectric layer is a thin 0.7Pb(Mg$_{1/3}$Nb$_{2/3}$)O$_3$-0.3PbTiO$_3$ (PMN-PT) [001]-cut single crystal with a record high piezoelectric coefficient, which also became feasible around the year 2000[21,22]. This configuration facilitates the conversion of the in-plane magnetostriction of the specimen into an electrical signal across the piezolayer. The magnetostriction (λ) measures the response of sample geometry in external magnetic fields, i.e., $\lambda(\mathbf{B}) = \Delta L(\mathbf{B})/L_0$, where L_0 is the sample length in zero magnetic field, and $\Delta L(\mathbf{B}) = L(\mathbf{B}) - L_0$ is the length change induced by magnetic field. Unlike traditional dc measurements, the ac ME method employs the ac-lock-in technique, which achieves an enhanced signal-to-noise ratio and high resolution by applying an ac-driven magnetic field ($\mathbf{B}_{ac}$). This technique has demonstrated high accuracy in characterizing magnetic skyrmion phases in materials such as MnSi[17] and Co$_7$Zn$_8$Mn$_5$[18], and in unveiling ferromagnetic spin-spin correlations in quasi-2D magnets, even within paramagnetic phases[19]. Hence, the ac ME method has the potential for detecting weak QOs in the magnetostriction of semimetals under moderate field and temperature conditions.

Theoretically, the ac ME technique can achieve superior resolution in detecting QOs of magnetostriction in semimetals with high frequencies. The real part of the ac voltage signal V_x is expected to be proportional to the piezomagnetic coefficient $\mu_0(\partial\lambda)/\partial B$ (where μ_0 is the permeability of vacuum)[23]. This derivative ($\partial\lambda/\partial B$) of the oscillatory part of magnetostriction can be estimated to be:

$$V_x \propto \frac{\partial\widetilde{\lambda}}{\partial B} \sim -\sum_r \frac{2\pi F_r}{B^2}\widetilde{\lambda}\left(\varphi_r + \frac{\pi}{2}\right) \qquad (1)$$

Where F_r is the oscillatory frequency and r is the index for it, φ_r is the corresponding oscillatory phase. This relation displays a phase shift of $\pi/2$ comparing to the original oscillatory magnetostriction, with an amplification factor of $2\pi F_r B^{-2}$. The B^{-2} part of this factor can significantly enhance the low-field oscillatory signals. The $2\pi F_r$ part of the factor provides a global enhancement to the oscillations, thus, high-frequency oscillations would be amplified further. On the other hand, the magnetostriction itself increases with decreasing F_r, i.e., with decreasing the size of the charge-carrier group[24]. Notably, for high frequencies above 100 T, the onset field for observing QOs may be significantly reduced since the amplification factor becomes even larger in lower magnetic fields.

In this study, we conducted an investigation on the nodal-line semimetal ZrSiS. We compared the ac composite ME method with four other techniques, including in-plane resistivity (ρ), out-of-plane magnetization ($\mathbf{M}$), out-of-plane magnetostriction λ, and in-plane thermopower (S), using the same thin ZrSiS single crystal. The measurements were carried out at temperatures down to 2 K and in magnetic fields up to 13 T. Our findings demonstrate that the ac ME method can effectively reveal all six fundamental frequencies while other methods cannot. Besides, results of the ME method display a series of magnetic breakdown frequencies around 8000 T with a low onset magnetic field of 7.6 T. And the

effective mass values of δ_1 and α bands can be determined from temperature-dependent data, showing nearly zero values. These results highlight the potential of the ME technique for exploring Dirac and Weyl physics as well as Fermi surface properties in other metals, under moderate experimental conditions.

RESULTS

Basic properties of ZrSiS
ZrSiS belongs to the WHM (W = Zr, Hf; H = Si, Ge, Sn, Sb; M = S, Se, Te) material system and crystallizes in the PbFCl structure type with a tetragonal *P4/nmm* space group (No. 129)[25], as depicted in Fig. 1a. The Si square net is situated in the *ab*-plane and is enclosed between Zr-S layers. X-ray diffraction analysis of a single crystal (inset of Fig. 1b) confirms the high quality of the ZrSiS samples. The diffraction pattern in Fig. 1b exhibits well-defined sharp (00 L) peaks, and the calculated *c*-axis lattice constant is 8.060 Å using the Nelson-Riley method, consistent with previous reports[26,27].

Figure 1c illustrates the temperature dependence of resistivity along the *a*-axis for two magnetic fields: 0 T and 8 T, where the field is aligned parallel to the *c*-axis. In the absence of a magnetic field, the resistivity shows typical metallic behavior, gradually decreasing as the temperature drops. The high quality of the crystal is evident from the calculated residual resistivity ratio of approximately 50. Conversely, in 8 T, a clear transition occurs, leading to a pronounced insulating behavior below 100 K. This field-induced crossover can be linked to the emergence of a band gap in topological semimetals, a phenomenon consistent with prior research[11].

Quantum oscillations in magnetic properties: magnetostriction and magnetization
As mentioned in various studies, the QOs are expected to be noticeable under high magnetic fields and low temperatures in different magnetic properties[10–16]. QOs in magnetostriction λ is a fundamental thermodynamic phenomenon that can directly reflect strain dependence of the Fermi surface. As depicted in Fig. 2a, field-dependent magnetostriction $\lambda(\mathbf{B})$ for both $\mathbf{B}$ and λ along the *c*-axis, exceeding 10^{-5} at 13 T, is measured with a capacitive dilatometer at 1.6 K. An oscillatory component with a minor amplitude (10^{-7}-10^{-8}) and low frequency is shown in the inset of Fig. 2a by subtracting a dominating linear background. The onset field of the oscillations is about 1.5 T. Other higher frequency oscillations reported in previous studies are not found in $\lambda(\mathbf{B})$ due to the thin crystal thickness (0.36 mm) and large background signal. In contrast, field-dependent magnetization $\mathbf{M}(\mathbf{B})$ (Fig. 2b) exhibits both low- and high-frequency oscillations. A similar dominant linear background is also identified while the onset field of the oscillations is reduced to 1 T, indicating better sensitivity in terms of QO. As a result, these two non-transport methods yield considerably less information within limited field and temperature condition compared to the known exotic features found in QO of ZrSiS appearing in high magnetic fields[10,15,16].

Quantum oscillations of ZrSiS in in-plane resistivity and thermopower
To show the QOs detected by transport properties, we measured the field-dependent resistivity ρ and thermopower S on the same crystal used in magnetic property measurements, as depicted in Figs. 2d, e, respectively. Field-dependent resistivity $\rho(\mathbf{B})$ (Fig. 2d) presents strong high-frequency and weak low-frequency oscillations. The dominant background of the ρ curve follows a B^2-like profile, which is common in metals. The substantial background raises its discernable onset field of oscillations to over 4 T.
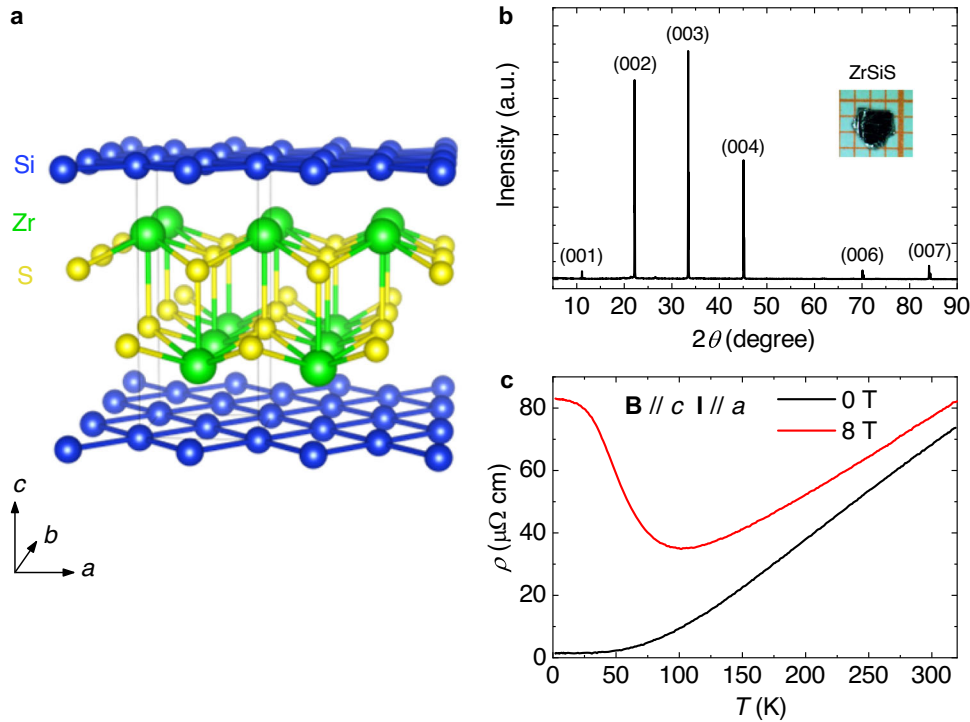
Fig. 1 Structure and basic sample characterizations of ZrSiS single crystal. a Schematic crystal structure of ZrSiS with $P4/nmm$ space group. **b** Single crystal X-ray diffraction pattern measured at room temperature. Inset: A photograph of ZrSiS single crystal. **c** Temperature-dependent resistivity under external magnetic fields of 0 and 8 T, applied along the c-axis.
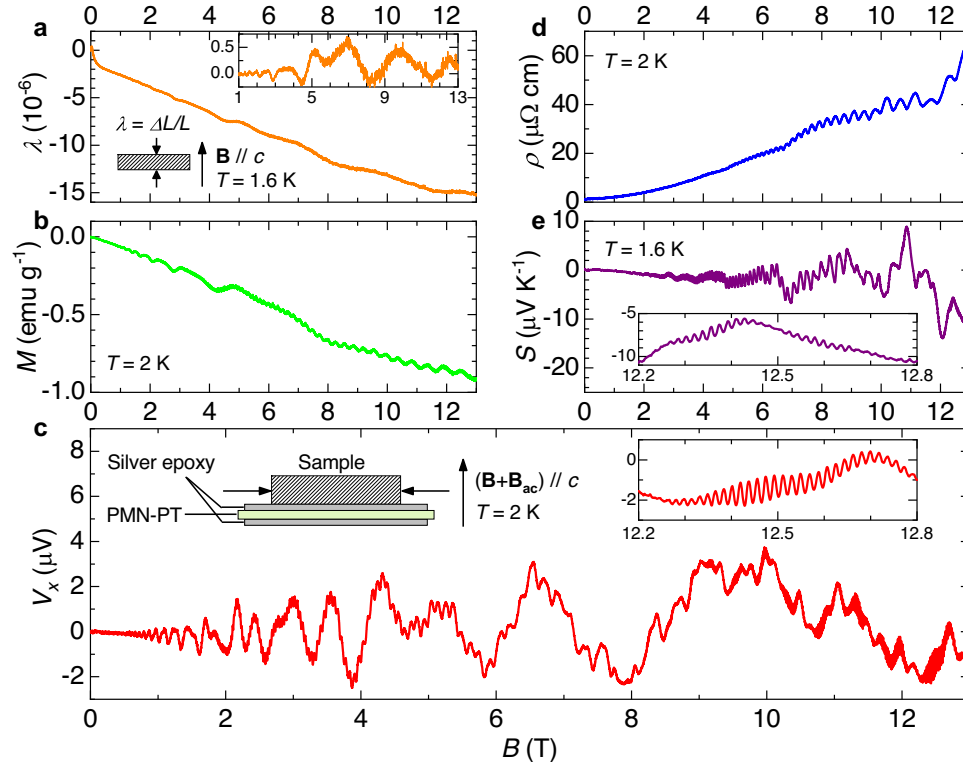

Fig. 2 Field dependent physical properties at ~2 K with B // c-axis. a Field-dependent magnetostriction along the c-axis ($L_0 = 0.36$ mm). Inset of (**a**) displays the oscillatory part with the background subtracted. **b** Field-dependent magnetization. **d** Field-dependent resistivity. **e** Field-dependent thermopower. Inset of (**e**) shows ultra-high-frequency oscillations in the field range above 12 T. **c** Real part of the ac voltage signal induced by in-plane deformation of the sample, which is adhered to PMN-PT. The deformation is stimulated by a sinusoidal magnetic field B_{ac} (left panel of inset of (**c**)). Right panel of inset of (**c**) shows ultra-high frequency oscillations in the field range above 12 T.
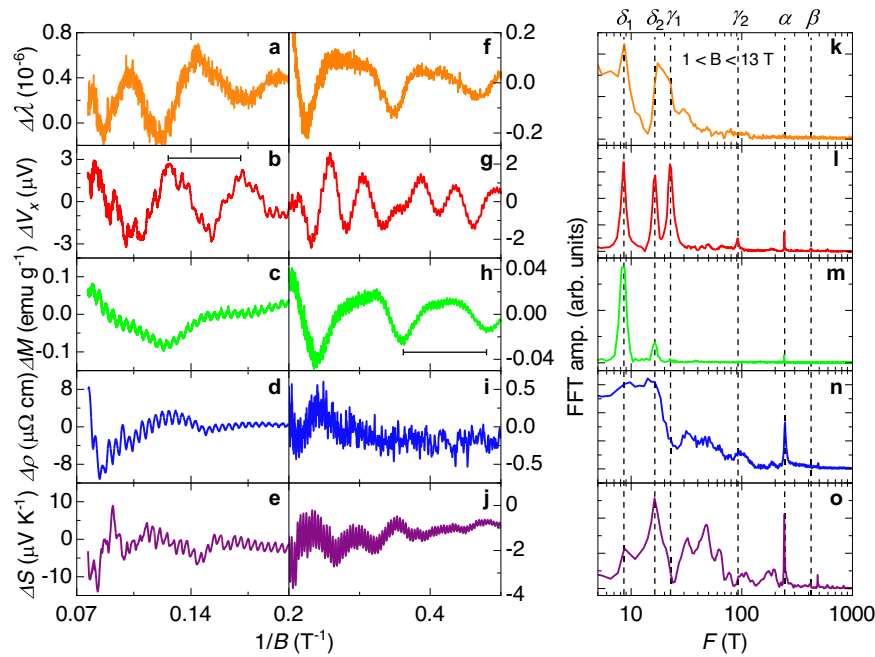
Fig. 3   1/B plots and FFT analyses of the oscillations of five physical properties. a–e 1/B plots ranging from 0.07 T^{-1} to 0.25 T^{-1} for five physical properties. Scale bar length in (**b**) is 1/22.5 T^{-1}, which implies a single period of $F(\gamma_1)$ oscillations. **f–j** 1/B plots for the same properties ranging from 0.25 T^{-1} to 0.8 T^{-1}. With a scale bar length of 1/8.5 T^{-1} in **h**, one single period of $F(\delta_1)$ oscillations can be revealed. **k–o** FFT analyses for each of the five physical properties. The analyses highlight six fundamental oscillatory frequencies in ZrSiS, indicated by six dotted lines.

Conversely, field-dependent thermopower S(**B**) at 1.6 K reveals more complex oscillations (Fig. 2e). Its background is much smaller than that of other methods. Consequently, its oscillation part shows an onset field of the oscillations as low as 1.5 T. The 8000 T QO, which has a relatively weak magnitude, appears around 8.7 T. The overall field-dependent profile of S(**B**) is consistent with previous studies[14].

Quantum oscillations of ZrSiS with composite magnetoelectric configuration

We found that the composite ME method exhibits a superior sensitivity compared to the above four methods. To employ the composite ME method on ZrSiS, we mechanically bonded the single crystal with a thin PMN-PT to produce a ZrSiS/PMN-PT laminate, as depicted in the inset of Fig. 2c. The real part of ME signal V_x as a function of the dc magnetic field **B** is measured at 2 K, as shown in Fig. 2c. QOs with various frequencies are displayed, revealing more details than the above four methods. V_x has a weak linear background, leading to a dominant oscillation signal as the magnetic field increases. The onset field of the oscillations drops to 0.5 T, which suggests that the oscillatory component of magnetostriction far exceeds the noise level. Additionally, V_x exhibits oscillations around 8000 T, as shown in the inset of Fig. 2c, similar to that in thermopower (inset of Fig. 2e). However, a lower starting field of 7.6 T is observed in the ME technique. Based on these features, the ME technique appears to be an excellent method for characterizing QOs.

Feature comparison and FFT analyses of QOs in ZrSiS

In this study, QOs measured by different methods are quantitatively analyzed. Fast Fourier transformation (FFT) analyses are employed to extract the oscillatory frequencies and amplitudes for each method, which are presented in Fig. 3k–o. The oscillations of various physical properties are plotted as a function of 1/B (inverse magnetic field) with the background subtracted. The entire field region is divided into two sections:

high field region (0.07 < 1/B < 0.2 T^{-1}, Fig. 3a–e) and low field region (0.2 < 1/B < 0.5 T^{-1}, Fig. 3f–j). For 1/B > 0.5 T^{-1}, the oscillation is too weak to be analyzed. The six fundamental frequencies are recognized by FFT in different field ranges in our ac ME method (Supplementary Note 1 and Supplementary Figure 1), and marked as dashed lines in the FFT plots. The discrepancies between different methods are revealed in the comparison. Oscillation frequencies of $F(\delta_1) \sim 8$ T and $F(\delta_2) \sim 16$ T are common among all the methods, except in resistivity where these two frequencies are not resolvable, as shown in Fig. 3n. $F(\gamma_1) \sim 22$ T appears to exist only in the oscillations of magnetostriction and ac ME signals (V_x), but the FFT peak in V_x is more pronounced than that in λ, with its onset field (~2.85 T) indicated in the low field region (Fig. 3g). $F(\gamma_2) \sim 91$ T is difficult to discern in any oscillation data directly, while only the FFT result of V_x (Fig. 3i) shows a discrete peak at this frequency. For the fundamental frequencies above 100 T, $F(\alpha) \sim 240$ T oscillations are common in these methods except in λ (Fig. 3l–o). $F(\beta) \sim 420$ T only appears in V_x, with the smallest amplitude in the FFT profile (Fig. 3l) compared to all the other fundamental frequencies.

It is noted that, in the high-field region (Fig. 3b) of V_x, the oscillations exhibit a complex pattern, indicating that more frequencies are included. The FFT analysis suggests a series of oscillations in the frequency range of 60 to 600 T (65, 183, and 593 T), which are combinations between $F(\alpha)$ and $F(\beta)$ orbits due to the magnetic breakdown phenomenon[16]. Only the 593 T frequency can be found in thermopower data as well (Fig. 3o). All these fundamental and breakdown frequencies below 1 kT are summarized in Table 1 and the frequencies above 1 kT will be discussed below. From Table 1, a combination of magnetostriction, resistivity, magnetization, and thermopower is insufficient to capture all the fundamental frequencies, and $F(\gamma_2)$ is still missing. In contrast, the ME method demonstrates an ultra-high-sensitive performance, independently revealing all the allowed frequencies reported previously[10–16].

Temperature-dependent QOs of V_x

We noticed that the effective mass m^* can be estimated by analyzing the temperature-dependent amplitude of ME QOs in FFT according to the Lifshitz-Kosevich formula[28]. Therefore, the field-dependent ME signals at selected temperatures are measured and depicted in Fig. 4a. A clear damping effect of oscillation amplitudes is revealed when the temperature increases from 2 to 20 K. The corresponding FFT amplitudes of the featured frequencies also reflect this tendency, as shown in Fig. 4b. $F(\delta_1)$ and $F(\alpha)$ are chosen to fit the thermal damping factor R_T in the conventional LK formula, as shown in Fig. 4c. Their temperature-dependent behaviors exhibit metallic fermion, and the effective masses are extracted to be $m^*(\delta_1) = 0.0357 \, m_0$ and $m^*(\alpha) = 0.0451 \, m_0$. Such small effective masses indicate nearly massless fermions for these two orbits, consistent with previous dHvA oscillation studies[13].

A series of ultra-high frequencies can also be observed in ME signals (Fig. 4d), which have been reported by magnetic torque and resistivity up to 35 T and down to 0.34 K[10,15,16]. The most pronounced peaks appear in a region of around 8.5 kT, labeled with six Roman numbers I to VI. The differences in frequency between these distinct peaks are $\sim F(\alpha)$ except the one between peaks IV and V, which is $\sim F(\beta) - F(\alpha)$. Two more peaks in a frequency region of around 11 kT are also detected but with much reduced amplitudes, and the difference between them is $\sim F(\alpha)$. The gap in

frequency between these two regions is indicated with a frequency of ~2330 T, whose origin is still controversial in the literatures[10,15,16]. We observed that the effective masses of orbits III and IV are fitted to be $m^*(III) = 0.124 \, m_0$ and $m^*(IV) = 0.159 \, m_0$, which hold the lowest magnitudes among these breakdown orbits (I to VI). This observation is based on their ability to persist at higher temperatures and their relatively higher amplitude compared to others. Notably, these effective masses are several times larger than those of the fundamental orbits. This significant increase in effective mass is indicative of a longer orbital length, which is a characteristic feature of giant breakdown orbits. These apparent features are overall consistent with the latest dHvA oscillation measurements[16], which further validate the high sensitivity of our method under moderate field and temperature conditions.

DISCUSION

It is noticeably that there are several pronounced peaks between 20 T to 80 T in Fig. 3o (thermopower), while they are small in other methods. We interpret these peaks as harmonics of the δ_2 frequency (~16 T), aligning with the analysis by Marcin Matusiak et al.[14], but we diverge from their interpretation, seeing the ~48 T frequency not as a new fundamental orbit but only as a third harmonic of δ_2. The heightened amplitude of these peaks can be explained by the spin damping factor R_s in LK formula:

$$R_s = \cos\frac{p\pi g m^*}{2m_0}. \tag{2}$$

Where p is harmonic index, g is the Landé g-factor. Adjusting R_s, can significantly alter the oscillatory amplitude of harmonic frequencies, sometimes even surpassing the fundamental frequency. Moreover, this effect varies between different measurement techniques. For instance, in $MoSi_2$ with magnetic field orientation **B** // [001], the dHvA oscillations[29] show higher amplitudes for the second harmonics compared to the fundamental frequencies. In contrast, the SdH oscillations[30] under the same conditions show much weaker second harmonics. Thus, in the ac composite ME technique and the other four methods, the smaller peaks in the 20–80 T range can be attributed to this method-varying effect of enhanced harmonic oscillations.
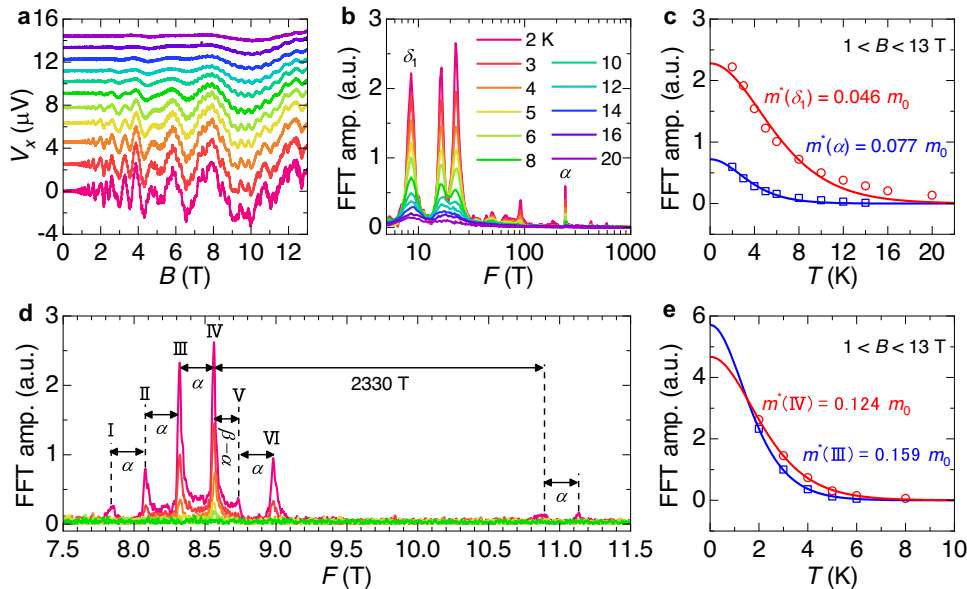
Table 1. Main oscillatory frequencies in FFT analyses for ZrSiS.

Method	Fundamental orbits						Breakdown orbits (<1000 T)		
	δ_1	δ_2	γ_1	γ_2	α	β	$2\alpha - \beta$	$\beta - \alpha$	$2\beta - \alpha$
λ	8.7	17.3	21.7						
V_x	8.5	16.5	22.4	91.6	242.0	419	65	183	593
M	8.5	16.4			241.1				
ρ		16.3			245.0				
S	8.7	16.3			241.6	419			594

Fig. 4 Field-dependent oscillations of V_x at selected temperatures and FFT analyses. a Background-subtracted field-dependent oscillations of V_x at selected temperatures with **B** // c. **b** FFT spectrum (5–1000 T) over a magnetic field range of 1–13 T. **c** Effective mass fitting of δ_1 and α orbits, revealing conventional metallic behavior consistent with the Lifshitz-Kosevich theory. **d** FFT spectrum (7.5–11.5 kT) across a magnetic field range of 1–13 T. **e** Effective mass fitting for orbitals III and IV.

We need to point out the limitation of our method. It would not be expected to work well for all types of materials. It tends to perform exceptionally well in non-magnetic metals, especially those that are multi-band and exhibit higher magnetostriction[24,31]. In metals and semimetals with magnetic orderings, the dominant magnetostriction signal from magnetic phases can overshadow the quantum oscillatory signals. This limitation also applies to type-II superconductors, where the vortex phase below the upper critical field can produce an overwhelmingly large signal[32], potentially masking the quantum oscillation signals in our method.

In summary, we have demonstrated that the ac composite ME method possesses high sensitivity for studying the complex QOs in the Dirac semimetal ZrSiS. In comparison to four other typical methods with the magnetic field and temperature limited to below 13 T and above 2 K, respectively, the QOs in the ME signal provide the most complete configuration of Fermi surfaces in ZrSiS with the lowest onset field ~0.5 T, whereas the combination of all four methods still lacks some of the allowed orbitals. In particular, FFT result of the ME oscillations yields a series of clearly separated peaks above 7.5 kT. Meanwhile, the effective masses of some orbitals can be obtained by studying the temperature-damping effect of the ME QOs. The outstanding performance of the ME method may stem from the additional factor introduced by $\partial\lambda/\partial B$. This factor shows significant enhancement when compared to directly measured magnetostriction. In terms of experimental techniques, the use of ac-driven and lock-in technique effectively reduces noise levels. As a result, our method enhances the sensitivity of probing quantum oscillations in magnetostriction. This increased sensitivity makes it practical for studying Dirac Fermions and other topological semimetals under moderate magnetic field and temperature conditions. This could pave the way for further investigations into Fermi surface behavior based on magnetostriction oscillations.

METHODS

Sample preparation

Single crystals of ZrSiS were synthesized by the chemical vapor transport method. The stoichiometric mixture of Zr (Alfa Aesar, 99.9%), Si (Alfa Aesar, 99.9%) and S (Alfa Aesar, 99.9%) powders were sealed in an evacuated quartz tube with I_2 being used as transport agent. The sealed quartz tubes were put in a two-zone tube furnace. The hot side is about 1020 °C and the cold side is 920 °C, and dwelled for two weeks. Plate-like shape single crystals with shinning surfaces were obtained. The size of the crystal is $2.72 \times 2.4 \times 0.36$ mm^3.

Transport measurements

Temperature dependent resistivity was measured using a four-probe method. All the measurements were done in a Quantum Design Physical Properties Measurement System (PPMS-9T) for $1.8 \, K < T < 400 \, K$ and $B < 9 \, T$.

Structural characterization

X-ray diffraction measurement of single crystal was performed by the PANalytical X'Pert diffractometer using the Cu K_α radiation ($\lambda = 0.15406$ nm) at room temperature.

Magnetization measurements

Magnetization measurements were conducted on oriented crystals in steady magnetic fields up to 14 T and at a temperature of 2 K. Either a commercial superconducting quantum interference device (SQUID) or a vibrating-sample-magnetometry from Quantum Design is used.

Striction measurements

High resolution magnetostriction measurements were achieved by using a capacitive dilatometer made of CuBe. To precisely measure the capacitance change, an Andeen Hagerling 2550 A ($f = 1$ kHz) capacitance bridge with driven voltage of 15 V was used.

Composite ME measurements

The setup for this method is illustrated in Fig. 2e. A PMN-PT [001]-cut single crystal, typically 0.2 mm thick, serves as a piezoelectric transducer to detect magnetostriction in the sample. Silver epoxy (H20E, EPO-TEK) is applied to function both as electrodes and as a binder. This configuration effectively converts the in-plane magnetostriction of the sample into a voltage signal with high conversion efficiency. To mitigate noise interference from our liquid-Helium-free cryostat and electrical sources, an ac lock-in technique is employed. A constant ac magnetic field (**B**$_{ac}$, approximately 0.5 Oe at a frequency of 211 Hz) is applied in conjunction with the static field **B**. This is achieved using a custom coil encircling the sample. The resulting piezoelectrically-induced ac voltage, with a resolution of approximately 0.1 μV, is captured using a lock-in amplifier (OE1022, SYSU Scientific Instruments). It is crucial to maintain a consistent relative positioning between the sample and the coil to avoid signal discrepancies.

Thermopower measurements

The thermopower S was measured along the a-axis of a single crystal with the magnetic field parallel to the c-axis. The sample is bridged over two oxygen-free copper blocks to generate a temperature difference. When measuring the quantum oscillations, heating power was held constant to maintain a temperature difference of ~0.5 K for the sample.

FFT analysis

These analyses were performed using the rectangle window function to prevent the modification of oscillatory amplitude. Appropriate field regions were chosen to ensure signal-to-noise ratio, with suitable zero padding to ensure resolution of the X-axis (frequency) of the results.

DATA AVAILABILITY

The data that support the findings of this study are available from the corresponding author upon reasonable request.

REFERENCES

1. Shoenberg, D. *Magnetic Oscillations in Metals. Cambridge Monographs on Physics* (Cambridge University Press, 1984).
2. de Haas, W. J. & van Alphen, P. M. The dependence of the susceptibility of diamagnetic metals upon the field. *Proc. Neth. R. Acad. Sci.* **33**, 1106 (1930).
3. Schubnikow, L. & de Haas, W. J. A new phenomenon in the change of resistance in a magnetic field of single crystals of bismuth. *Nature* **126**, 500 (1930).
4. Wu, Y. et al. Dirac node arcs in PtSn$_4$. *Nat. Phys.* **12**, 667–671 (2016).
5. Bian, G. et al. Topological nodal-line fermions in spin-orbit metal PbTaSe$_2$. *Nat. Commun.* **7**, 10556 (2016).
6. Schoop, L. M. et al. Dirac cone protected by non-symmorphic symmetry and three-dimensional Dirac line node in ZrSiS. *Nat. Commun.* **7**, 11696 (2016).
7. Neupane, M. et al. Observation of topological nodal fermion semimetal phase in ZrSiS. *Phys. Rev. B* **93**, 201104 (2016).
8. Takane, D. et al. Dirac-node arc in the topological line-node semimetal HfSiS. *Phys. Rev. B* **94**, 121108 (2016).
9. Hosen, M. M. et al. Tunability of the topological nodal-line semimetal phase in ZrSiX-type materials (X = S, Se, Te). *Phys. Rev. B* **95**, 161101(R) (2017).

10. Pezzini, S. et al. Unconventional mass enhancement around the Dirac nodal loop in ZrSiS. *Nat. Phys.* **14**, 178 (2018).

11. Singha, R., Pariari, A. K., Satpati, B. & Mandal, P. Large nonsaturating magnetoresistance and signature of nondegenerate Dirac nodes in ZrSiS. *Proc. Natl Acad. Sci. USA* **114**, 2468 (2017).

12. Ali, M. N. et al. Butterfly magnetoresistance, quasi-2d Dirac Fermi surface and topological phase transition in ZrSiS. *Sci. Adv.* **2**, e1601742 (2016).

13. Hu, J. et al. Nearly massless Dirac fermions and strong Zeeman splitting in the nodal-line semimetal ZrSiS probed by de Haas–van Alphen quantum oscillations. *Phys. Rev. B* **96**, 045127 (2017).

14. Matusiak, M., Cooper, J. & Kaczorowski, D. Thermoelectric quantum oscillations in ZrSiS. *Nat. Commun.* **8**, 15219 (2017).

15. Orbanić, F. et al. Quantum oscillations of the magnetic torque in the nodal-line Dirac semimetal ZrSiS. *Phys. Rev. B* **103**, 045122 (2021).

16. Müller, C. S. A. et al. Determination of the Fermi surface and field-induced quasiparticle tunneling around the Dirac nodal loop in ZrSiS. *Phys. Rev. Res.* **2**, 023217 (2020).

17. Chai, Y. et al. Probe of skyrmion phases and dynamics in MnSi via the magnetoelectric effect in a composite configuration. *Phys. Rev. B* **104**, L100413 (2021).

18. Zeng, H. et al. Magnetic and transport properties of chiral magnet $Co_7Zn_8Mn_5$. *J. Magn. Magn. Mater.* **560**, 169631 (2022).

19. Zhang, Y. et al. Observation of enhanced ferromagnetic spin-spin correlations at a triple point in quasi-two-dimensional magnets. *Phys. Rev. B* **107**, 134417 (2023).

20. Ryu, J., Priya, S., Uchino, K. & Kim, H.-E. Magnetoelectric effect in composites of magnetostrictive and piezoelectric materials. *J. Electroceram.* **8**, 107–119 (2002).

21. Luo, H., Xu, G., Wang, P. & Yin, Z. Growth and characterization of relaxor ferroelectric PMNT single crystals. *Ferroelectrics* **231**, 97 (1999).

22. Bokov, A. A. & Ye, Z.-G. Ferroelectric properties of monoclinic $Pb(Mg_{1/3}Nb_{2/3})O_3$-$PbTiO_3$ crystals. *Phys. Rev. B* **66**, 094112 (2002).

23. Burdin, D. A., Chashin, D. V., Ekonomov, N. A. & Fetisov, Y. K. Static deformation of a ferromagnet in alternating magnetic field. *J. Magn. Magn. Mater.* **406**, 217 (2016).

24. Cichorek, T., Bochenek, Ł., Juraszek, J., Sharlai, Y. V. & Mikitik, G. P. Detection of relativistic fermions in Weyl semimetal TaAs by magnetostriction measurements. *Nat. Commun.* **13**, 3868 (2022).

25. Klein Haneveld, A. J. & Jellinek, F. Zirconium silicide and germanide chalcogenides preparation and crystal structures. *Rec. Trav. Chim. Pays-Bas* **83**, 776 (1964).

26. Singha, R. et al. Probing lattice dynamics and electron–phonon coupling in the topological nodal-line semimetal ZrSiS. *Phys. Rev. B* **97**, 094112 (2018).

27. Sankar, R. et al. Crystal growth of Dirac semimetal ZrSiS with high magnetoresistance and mobility. *Sci. Rep.* **7**, 40603 (2017).

28. Kaneta-Takada, S. et al. High-mobility two-dimensional carriers from surface Fermi arcs in magnetic Weyl semimetal films. *npj Quant. Mater.* **7**, 102 (2022).

29. van Ruitenbeek, J. M. et al. de Haas–van Alphen effect in $MoSi_2$. *Phys. Rev. B* **35**, 7936 (1987).

30. Pavlosiuk, O., Swatek, P. W., Wang, J.-P., Wiśniewski, P. & Kaczorowski, D. Giant magnetoresistance, Fermi-surface topology, Shoenberg effect, and vanishing quantum oscillations in the type-II Dirac semimetal candidates $MoSi_2$ and WSi_2. *Phys. Rev. B* **105**, 075141 (2022).

31. Michenaud, J.-P., Heremans, J., Shayegan, M. & Haumont, C. Magnetostriction of bismuth in quantizing magnetic fields. *Phys. Rev. B* **26**, 2552–2559 (1982).

32. Lu, P., et al. Comprehensive characterizing of vortex phases in type-II superconductor $YBa_2Cu_3O_7$-x by a magnetoelectric technique. Preprint at https://arxiv.org/abs/2111.07287 (2021).

AUTHOR CONTRIBUTIONS

Y.S.C. and X.L. initiated the project. Y.W. grew the crystals. L.Z, and Y.G.Z. measured the MES, resistivity, and magnetization. S.L. measured the magnetostriction. L.Z. and Y.S.C. analyzed the results, interpreted them, and put them into context. Y.S.C. and X.L. supervised the research. All authors discussed the results and contributed to writing the manuscript.

COMPETING INTERESTS

The authors declare no competing interests.

ADDITIONAL INFORMATION

Supplementary information The online version contains supplementary material available at https://doi.org/10.1038/s41535-024-00622-w.

Correspondence and requests for materials should be addressed to Xuan Luo or Yisheng Chai.

Reprints and permission information is available at http://www.nature.com/reprints

Publisher's note Springer Nature remains neutral with regard to jurisdictional claims in published maps and institutional affiliations.